Optica Applicata, Vol. XLVIII, No. 1, 2018
DOI: 10.5277/oa180107

Manipulation of the supercontinuum energy distribution based on the positive chirp in photonic crystal fiber

HUA YANG*, XIONGFENG TONG, SAILI ZHAO, YING HUANG

Key laboratory for Micro/Nano Optoelectronic Devices of Ministry of Education,
College of Computer Science and Electronic Engineering,
Hunan University, Changsha 410082, China

*Corresponding author: huayang@hnu.edu.cn

The effect of initial frequency chirp is numerically investigated to obtain high-efficient supercontinuum radiation in photonic crystal fibers with two closely spaced zero-dispersion wavelengths. Our results show that the positive chirp can significantly improve the probability of energy transferred from the soliton to the dispersive wave. And with the increase of the chirp, the energy increases obviously. At the same time, the intensity of the dispersive wave is proportional to the chirp value. Especially, solitons will not appear when the chirp value exceeds 3.9. Therefore, choosing an appropriate positive chirp, we can regulate the energy of the dispersive wave and solitons in photonic crystal fibers.

Keywords: chirp, dispersive waves, solitons.

1. Introduction

Since its first observation by RANKA *et al*. [1], supercontinuum (SC) generation in photonic crystal fibers (PCFs) has remained a subject of extensive research. The invention of PCFs has opened a new horizon for effective SC generation because of its "endless single-mode" behavior, and controllable dispersion characteristics as well as excellent nonlinear properties [2–4]. When a femtosecond optical pulse pumped in the anomalous dispersion regime of PCFs, the Raman scattering and high-order dispersion effects are two prominent factors that greatly affect the ideal periodic high-order soliton evolution [5, 6]. Consequently, the soliton-related dynamics such as soliton fission, dispersive wave (DW) generation, and soliton trapping [5, 7–13] contribute to a broadband SC generation.

During the soliton fission, the DW is emitted in the normal dispersion regime due to the energy transferred from soliton to narrow-band resonance [6–10]. The wavelength of DW is red shift or blue shift with respect to the soliton central wavelength according to the phase-matching condition between DW and the soliton [6, 14, 15]. It

is well known that main contribution to the spectrum position of the DW is due to the dispersion slope, *i.e*. third-order dispersion (TOD) [16, 17]. When soliton propagates in the anomalous dispersion region, *i.e*., if $\beta_3 > 0$, the DW is emitted on the blue side (B-DW) and it travels slower than the Raman soliton. While, if $\beta_3 < 0$, the DW is emitted on the red side (R-DW) and travels faster than the Raman soliton [18–20]. Many analysis and experimental studies have been carried out in PCFs in order to better understand the underlying mechanisms in the process of SC generation. The effects from input pulse parameters such as pulse energy, peak power, pulse duration, and central wavelength on the SC generation have been investigated thoroughly [5]. In [21], the mechanism of soliton trapping is disclosed in PCF with two zero-dispersion wavelengths (ZDWs). The role of chirp on soliton trapping of DWs is also unfolded in PCF with two ZDWs [22]. However, to the best of our knowledge, the influence of positive chirp on the energy redistribution between soliton and DWs has not been studied in PCFs in detail. In this paper, we adopt numerical methods to simulate the influence of positive chirp on the SC generation and DWs' energy in PCF with two ZDWs in detail. These results indicate that a positive initial chirp accelerates the energy transferred to the normal dispersion regime by affecting self-phase modulation (SPM) and four-wave mixing (FWM) processes. The energy of DW and stability of optical solitons can be controlled if the chirp does not exceed a critical value. Positive chirp induces the energy redistribution between the soliton and DWs, thus the intensity of R-DWs and B-DWs is proportional to the chirp value. Therefore the spectral bandwidth and spectral flatness are enhanced in the process of SC generation.

This paper is organized as follows. In Section 2, the theoretical model with nonlinear and high-order dispersion effects is introduced when ultra-short pulse propagates in PCF. In Section 3, detailed discussion under varied chirp is presented during SC and DW generation. Finally, a conclusion is made based on the above results.

2. Numerical model

When an ultra-short pulse is propagating in PCF, the generalized nonlinear Schrödinger equation (GNLSE) is used as the propagation model:

$$\frac{\partial A(z,T)}{\partial z} = \sum_{k\geq 2} \frac{i^{k+1}\beta_k}{k!}\frac{\partial^k A}{\partial T^k} + i\gamma\left(1+\frac{i}{\omega_0}\frac{\partial}{\partial T}\right)\left[A(z,t)\int_{+\infty}^{-\infty} R(T')\left|A(z,T-T')\right|^2 \mathrm{d}T'\right] \tag{1}$$

where $A(z, T)$ is the pulse envelope and T is a delayed time parameter measured in the reference frame moving with the envelop group velocity at the pump frequency. The first term on the right-hand side of Eq. (1) refers to the dispersion effect in PCF and β_k is the k-th order dispersion coefficient by performing a Taylor-series expansion of propagation constant around a center frequency ω_0; the second term represents non-

linear effects, where γ denotes the nonlinear coefficient. The nonlinear response $R(t) = (1 - f_R)\sigma(t) + f_R h_R(t)$ with $f_R = 0.18$ includes instantaneous and delayed Raman contributions, and the response h_R used here is the same as the analytic approximations in [6]. The fiber loss is neglected since only a short length of the fiber is considered in the simulations. We adopt the chirped hyperbolic-secant pulses in the numerical simulation, where the input pulses are assumed to have the form:

$$A(z, T) = \sqrt{P_0}\ \mathrm{sech}\left(\frac{T}{T_0}\right)\exp\left(-\frac{iCT^2}{2T_0^2}\right) \tag{2}$$

where P_0 is the peak power and T_0 is related to the FWHM with $T_{FWHM} \approx 1.763T_0$, and C is the initial linear frequency chirp parameter as it appears in the simulations. We employ the standard split-step Fourier method to numerically solve the GNLSE [6]. To observe the visual results, we simulate the pulse in the time and spectral domain simultaneously by using the well-known X-FROG (cross-correlation frequency resolved optical gating) spectrograms [13, 23–27]. Intuitive images of the pulse evolution are obtained by plotting spectrograms as the pulse propagates in the fiber. In this paper, the spectrograms are numerically simulated with a windowed Fourier transform of the field envelope:

$$S(t, \omega) = \left|\int_{-\infty}^{+\infty} \mathrm{d}t' A_{\mathrm{ref}}(t' - t)A(t')\exp(-i\omega t)\right|^2 \tag{3}$$

Here, A_{ref} denotes an envelope of the reference pulse, and A represents the envelope of the field inside the PCF. We choose the pump pulse as the reference pulse. In addition, we plot the spectrograms on the same logarithmic color scale.

3. Numerical results and discussions

On the basis of the GNLSE, a detailed analysis is presented on SC and DW generation under various positive chirps, where soliton fission mechanisms play an important role. The dispersion profile and relative group delay are presented as a function of the wavelength from [21], where the two ZDWs are located at 650 and 930 nm. The dispersion regime between the two ZDWs is anomalous while the others are normal [25]. The dispersion slope in the vicinity of the second ZDW is negative, whereas it is positive near the first ZDW. In this paper, the input pulse parameters are used in our numerical simulations as follows: the pump wavelength $\lambda_0 = 725$ nm, initial pulse width $T_0 = 50$ fs, and the fiber length is 600 cm.

By providing a large spectral overlap, the pump energy can be efficiently shed away to DW in the normal dispersion region of the PCF. The center frequencies of DW are determined by the phase-matching condition [5, 15, 26]

$$\Delta\beta = \beta(\omega_p) - \beta(\omega_{DW}) = (1 - f_R)\gamma(\omega_p)P_p - \sum_{n \geq 2}^{n=15} \frac{\omega_{DW} - \omega_p}{n!}\beta_n(\omega_p) \quad (4)$$

where $\beta(\omega_p)$ and $\beta(\omega_{DW})$ represent the propagation constants at the angular frequency of the pump (ω_p) and the dispersive wave (ω_{DW}), respectively; $\beta_n(\omega_p)$ denotes the high -order dispersion parameters. The factor f_R accounts for the fractional contribution of the Raman delayed response in the fiber and P_p is the peak power of the pump.

In order to better understand the role of chirp effect in the process of the DW and soliton generation, we firstly present the temporal evolution of the input pulses with different initial chirp coefficients propagating in the 0.6 m PCF. As shown in Figs. 1**a**–1**c**, we can see how the SC temporal intensity is affected due to different chirps. In the time domain, several red-shifted Raman solitons can be observed and its temporal delays increase with the increase of chirp. In this case, the delay of the input pulse depends on the chirp. By comparing the three figures, we find that input pulses with larger C value have longer delay. After the initial compression stage, the soliton undergoes fission resulting from the higher-order dispersion and nonlinear effects, and then the pulse breaks up into a series of fundamental solitons accompanied by emission of non-soliton radiation as shown in Fig. 1. With the increase of the chirp, the pulse reaches the fission stage earlier, so the soliton is ejected earlier and experiences large delay [22, 28, 29]. This explains why the DW is emitted earlier in Fig. 1**c** compared with that in Figs. 1**a** and 1**b**. In addition, the first-ejected soliton exhibits a stronger intensity and experiences a larger delay.

We now show how the SC varies over a wide range of chirp. Figures 2**a**–2**c** show the corresponding spectral evolution in the same PCF. In the frequency domain, the pulse exhibited symmetric spectral broadening as a result of SPM at the distance less than 40 cm in Figs. 2**a**–2**c**. Subsequently, as the injected pulse attains its maximum bandwidth after strong temporal compression, the high-order soliton breaks up into

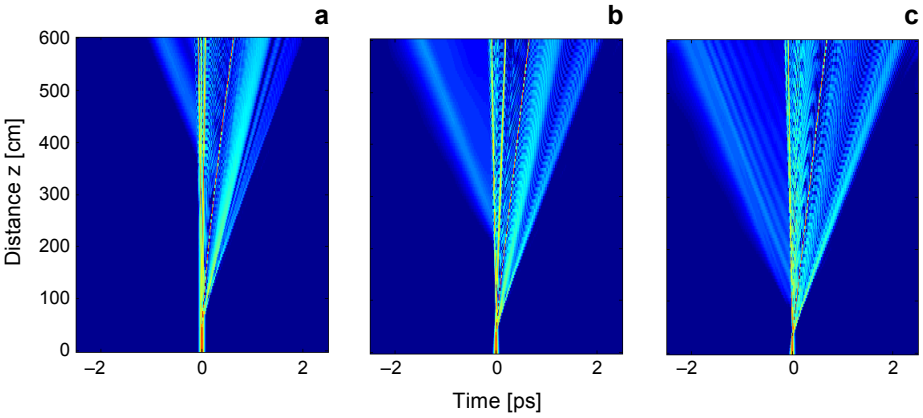

Fig. 1. Temporal evolution with different input chirp signatures; $C = 0$ (**a**), $C = 2$ (**b**), and $C = 3.9$ (**c**).

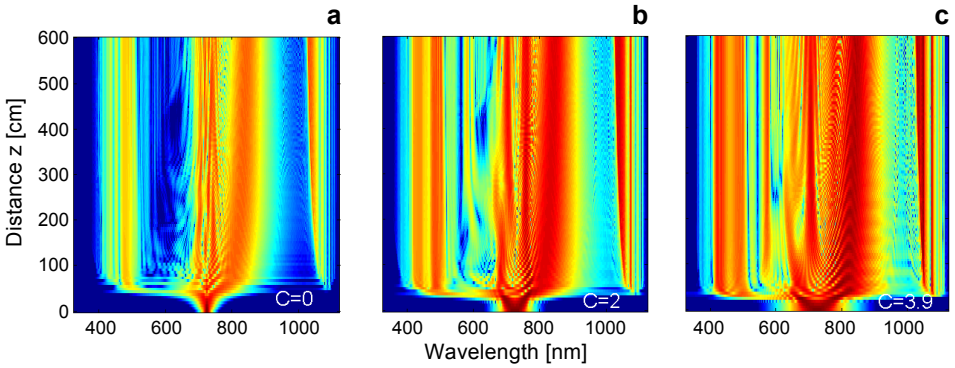

Fig. 2. Spectral evolution with different input chirp signatures; $C = 0$ (**a**), $C = 2$ (**b**), and $C = 3.9$ (**c**).

a series of fundamental solitons with different widths and peak intensity due to dispersion and Raman perturbation. Then, the spectrum becomes asymmetric. As the solitons experience Raman induced frequency shift (RIFS), B-DW is excited when meeting the phase-matched condition. Besides, the B-DW can be amplified by the energy transferred from soliton [13, 30].

Figure 2**a** shows the spectral evolution when $C = 0$. In this case, the initial spectral broadening is induced by SPM, which is followed by the onset of soliton fission. From this figure, we see that a fundamental soliton and DW is generated when the propagation distance is about 50 cm. And we note that as the central frequency of red-shift soliton gradually approaches the second ZDW with a negative dispersion slope, R-DW is excited at about 100 cm. We can see the R-DWs as well as B-DWs are both located at the normal dispersion regime and thus the SC is bounded by the two branches of DWs. With further propagation, the red-shift soliton suddenly ceases to shift in the vicinity of the second ZDW due to the balance of RIFS and the spectral recoiling effect. The above phenomena are consistent with the Ref. [21]. However, the intensity of DWs is relatively weaker compared with those shown in Figs. 2**b** and 2**c**. As we known, the intensity of the DW is related to the energy transferred from the soliton to DW.

As the chirp coefficient increases, we find some interesting phenomena in Figs. 2**b** and 2**c**, respectively. *i*) The larger the chirp, the bigger the spectrum broadening. *ii*) R-DW is excited at a shorter propagation distance and the intensity of R-DWs increases more at the end of the fiber when chirp increases. *iii*) The chirp can dramatically influence the spectral recoiling. This is mainly because SPM and FWM can be facilitated by employing positive chirps. The energy can be transferred to the normal dispersion region from the region within the two zero-dispersion wavelengths provided that the initial positive chirp is considered. It also reveals that the coupling between the DW and Raman soliton may be a key mechanism in controlling the spectral broadening under suitable chirp conditions.

In Figures 3**a** and 3**b**, the fundamental soliton and DW is not strong in a shorter propagation distance. But with the increase of the propagation distance, the higher-order soliton broke up into red-shifted fundamental solitons through soliton fission. During

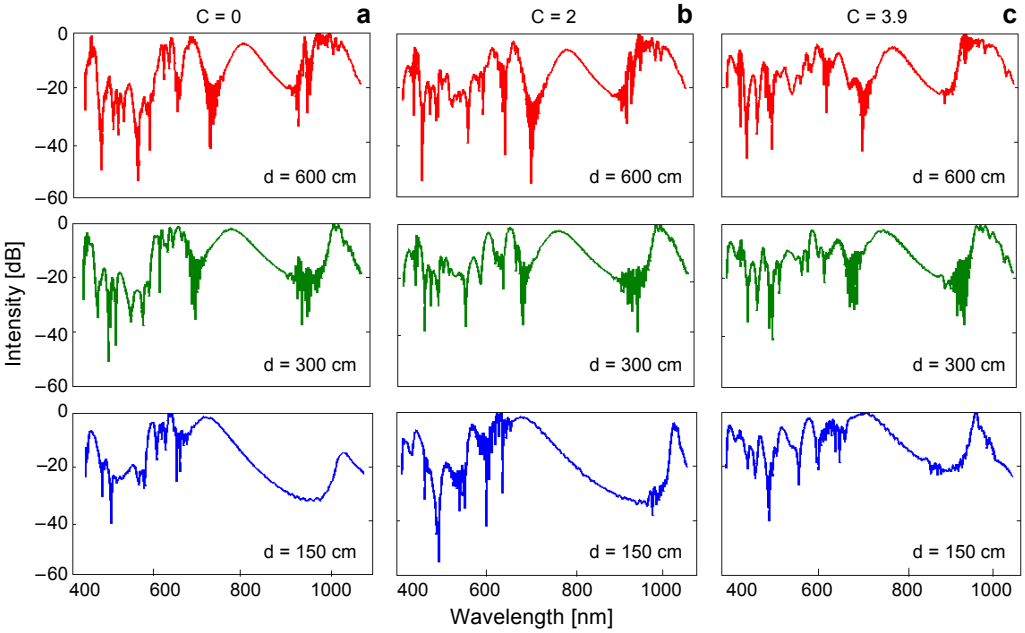

Fig. 3. Evolution of the spectral signatures as a function of fiber length pumped at 725 nm with different C coefficients: $C = 0$ (**a**), $C = 2$ (**b**), and $C = 3.9$ (**c**). Besides, the spectrum evolution at various propagating distances of 600, 300, and 150 cm.

the soliton fission, DW is emitted due to the energy transferred from soliton to narrow -band resonance in the normal dispersion regime. More importantly, we can see that the amplitude and the shape of the soliton are not changed at the propagating distance $d = 300$ cm and $d = 600$ cm. The oscillation of spectrum can be found at 700 –850 nm in Figs. 3**c**. In other words, soliton has an oscillation behavior and began to become unstable [31]. With the increase of chirp, we find that the oscillation becomes more intense. The large chirp can simply be detrimental because it superimposes on the SPM-induced chirp and disturbs the exact balance between the group velocity dispersion (GVD) and SPM effects necessary for the soliton formation [32, 33]. Formation of a soliton is expected for small values of C because solitons are generally stable under weak perturbations. However, a soliton is destroyed if C exceeds a critical value C_{cr}. The critical value can be obtained with the inverse scattering method [34]. The real and imaginary parts of the eigenvalues (EVs) correspond to relative soliton velocities and amplitudes. As the chirp increases, the EVs move toward zero, showing that the solitons are less energetic. So, solitons exist as long as the imaginary part of EV is positive, which is a gradual process. With the increase of the chirp, the balance for the soliton formation is broken slowly. When C increases to a critical value C_{cr}, the oscillation becomes more intense, and the stability of the soliton will be destroyed. Our nu-

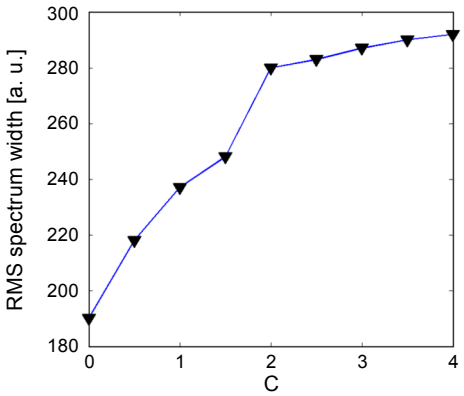

Fig. 4. RMS spectrum width varied along with chirp.

merical simulations indicate that the energy of DW and stability of optical solitons can be controlled if the chirp does not exceed 3.9.

The effect of initial chirp on the spectrum width of the output pulse is shown in Fig. 4, which plots the root mean square (RMS) spectrum width as a function of chirp parameter. In this case, the bandwidth of the output pulse depends on the initial chirp. Input pulses with larger chirp value lead to output pulses with broader bandwidths. Some important features can be found in Fig. 4. The spectrum bandwidth of the output pulse increases dramatically when the chirp increases from 0 to 2. Then the bandwidth is increased slightly after the chirp is larger than 2. All in all, it is important to choose an appropriate chirp, which cannot only ensure the stability of soliton, but also be beneficial to get the maximum output bandwidth.

In order to clearly show the process of soliton trapping DW by chirp along with the pulse evolution, a short propagation distance is chosen in our numerical simulations. The evolution of the numerical spectrogram for various values of propagation lengths z is plotted in Fig. 5. In Figures 5**a**–5**c**, spectrogram traces of 50 fs input pulse with $C = 0$ at fiber length of 60, 150 and 300 cm are showed, respectively. While in Figs. 5**d**–5**f** the $C = 2$ and other parameters are the same. When the propagation distance is about 0–60 cm in Figs. 5**a** and 5**d**, the first-ejected soliton is not stable due to high-order dispersion and nonlinear effects. Then, the soliton sheds away energy to B-DWs located at the short-wavelength edge of spectrum. Initially, the wavelength of the pump pulse is close to the smaller ZDW, which gives rise to a strong amplification of the B-DWs. In Figs. 5**b** and 5**e**, the first-ejected soliton continually experiences soliton self-frequency shifting (SSFS) due to RIFS and then B-DWs can be continually amplified. And in Fig. 5**b** there is little energy contained in the R-DWs compared with that in Fig. 5**e**. When the center wavelength of the soliton shifts to the vicinity of the higher ZDW, the R-DW starts to be amplified. In Figs. 5**c** and 5**f**, we can find that for the pulse with chirp, the intensity of R-DW and B-DW is stronger compared with that without chirp,

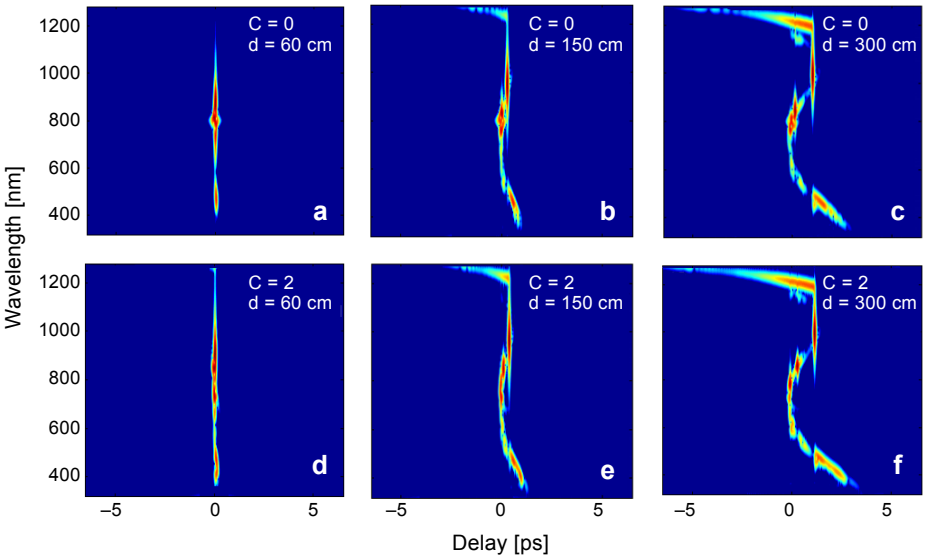

Fig. 5. The numerical X-FROG traces of the 50 fs pulse for different propagation lengths of 60, 150, and 300 cm for $C = 0$ (**a**–**c**), and of 60, 150, and 300 cm, for $C = 2$ (**d**–**f**).

because the positive chirp can improve the probability of the transferred energy from the soliton to DW. However, with further propagation the central wavelength of the soliton remains unchanged because a balance is achieved between stimulated Raman scattering (SRS) and spectral recoiling.

In Figure 6, the intensity proportion of DW is plotted with the varied chirp. As C changes from 0 to 3.9, the power ratio of R-DWs changes from 54.3% to 58.5%,

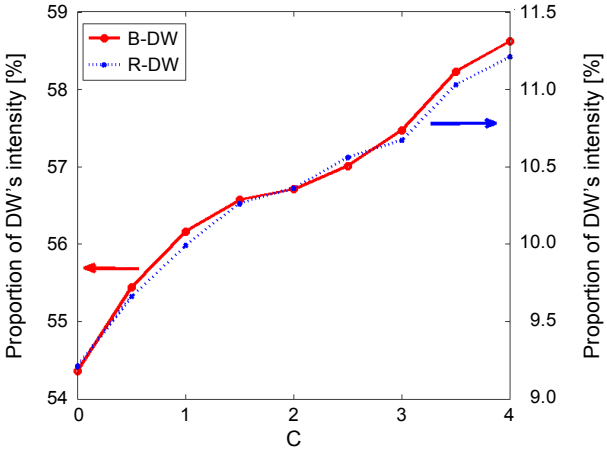

Fig. 6. The proportion of DW's intensity with varied chirp.

while the B-DWs relatively slightly, just from 9.2% to 11.3%. It is clear that with the increase of *C* coefficient, the energy of DWs increases greatly. This is because the positive chirp can significantly improve the efficiency of the energy transferred from the soliton to DWs, and the intensity of R-DWs and B-DWs can both be dramatically influenced. In a word, the intensity of the DWs is proportional to the chirp value. So the energy of DWs and stability of solitons in PCF can be manipulated by positive chirp.

4. Conclusions

In this work, we have numerically investigated the possibility of controlling the SC and DW generation by positive chirp. The SC spectral shape can be significantly modified at optimal input parameters. A small chirp value is a benefit to the formation of a soliton, and a soliton is destroyed if the chirp exceeds a critical value. Our numerical simulations indicate that the energy of DWs and stability of optical solitons can be controlled. Our result also shows that positive chirp induces the energy redistribution between soliton and DWs, thus the intensity of R-DWs and B-DWs is proportional to the chirp value. So we can manipulate the energy distribution of DWs and stability of solitons in PCF by positive chirp.

Acknowledgements – This work was supported by the National Natural Science Foundation of China under Grant 61275137 and the National Natural Science Foundation of China under Grant 61571186.

References

[1] Ranka J.K., Windeler R.S., Stentz A.J., *Visible continuum generation in air–silica microstructure optical fibers with anomalous dispersion at 800 nm*, Optics Letters **25**(1), 2000, pp. 25–27.
[2] Russell P.J., *Photonic crystal fibers*, Science **299**(5605), 2003, pp. 358–362.
[3] Knight J.C., *Photonic crystal fibers*, Nature **424**(17), 2003, pp. 847–851.
[4] Reeves W.H., Skryabin D.V., Biancalana F., Knight J.C., Russell P.St.J., Omenetto F.G., Efimov A., Taylor A.J., *Transformation and control of ultra-short pulses in dispersion-engineered photonic crystal fibers*, Nature **424**(6948), 2003, pp. 511–515.
[5] Dudley J.M., Genty G., Coen S., *Supercontinuum generation in photonic crystal fiber*, Reviews of Modern Physics **78**(4), 2006, pp. 1135–1184.
[6] Agrawal G.P., *Nonlinear Fiber Optics*, 4th Ed., Academic Press, 2007.
[7] Demircan A., Pietrzyk M., Bandelow U., *Effects of higher-order dispersion on pulse splitting in the normal dispersion regime*, Optical and Quantum Electronics **40**(5–6), 2008, pp. 455–460.
[8] Taylor J.R., *Supercontinuum Generation in Optical Fibers*, Cambridge University, London, 2010.
[9] Skryabin D.V., Yulin A.V., *Theory of generation of new frequencies by mixing of solitons and dispersive waves in optical fibers*, Physical Review E **72**(1), 2005, article ID 016619.
[10] Gorbach A.V., Skryabin D.V., Stone J.M., Knight J.C., *Four-wave mixing of solitons with radiation and quasi-nondispersive wave packets at the short-wavelength edge of a supercontinuum*, Optics Express **14**(21), 2006, pp. 9854–9863.
[11] Chu Liu, Rees E.J., Laurila T., Shuisheng Jian, Kaminski C.F., *Periodic interaction between solitons and dispersive waves during the generation of non-coherent supercontinuum radiation*, Optics Express **20**(6), 2012, pp. 6316–6324.

[12] TRAVERS J.C., RULKOV A.B., CUMBERLAND B.A., POPV S.V., TAYLOR J.R., *Visible supercontinuum generation in photonic crystal fibers with a 400 W continuous wave fiber laser*, Optics Express **16**(19), 2008, pp. 14435–14447.
[13] HILL S., KUKLEWICZ C.E., LEONHARDT U., KÖNIG F., *Evolution of light trapped by a soliton in a microstructured fiber*, Optics Express **17**(16), 2009, pp. 13588–13601.
[14] FROSZ M.H., FALK P., BANG O., *The role of the second zero-dispersion wavelength in generation of supercontinua and bright-bright soliton-pairs across the zero-dispersion wavelength*, Optics Express **13**(16), 2005, pp. 6181–6192.
[15] GENTY G., LEHTONEN M., LUDVIGSEN H., *Effect of cross-phase modulation on supercontinuum generated in microstructured fibers with sub-30 fs pulses*, Optics Express **12**(19), 2004, pp. 4614–4624.
[16] ROY S., BHADRA S.K., AGRAWAL G.P., *Perturbation of higher-order solitons by fourth-order dispersion in optical fibers*, Optics Communications **282**(18), 2009, pp. 3798–3803.
[17] DAJUN LEI, HUI DONG, SHUANGCHUN WEN, HUA YANG, *Manipulating dispersive wave generation by frequency chirp in photonic crystal fibers*, Journal of Lightwave Technology **27**(20), 2009, pp. 4501–4507.
[18] HUA YANG, FANG HAN, HUI HU, WEIBIN WANG, QILIN ZENG, *Spectral-temporal analysis of dispersive wave generation in photonic crystal fibers of different dispersion slope*, Journal of Modern Optics **61**(5), 2014, pp. 409–414.
[19] SAILI ZHAO, HUA YANG, NENGSONG CHEN, CHUJUN ZHAO, *Controlled generation of high-intensity optical rogue waves by induced modulation instability*, Scientific Reports **7**, 2017, article ID 39926.
[20] SAILI ZHAO, HUA YANG, CHUJUN ZHAO, YUZHE XIAO, *Harnessing rogue wave for supercontinuum generation in cascaded photonic crystal fiber*, Optics Express **25**(7), 2017, pp. 7192–7202.
[21] WEIBIN WANG, HUA YANG, PINGHUA TANG, CHUJUN ZHAO, JING GAO, *Soliton trapping of dispersive waves in photonic crystal fiber with two zero dispersive wavelengths*, Optics Express **21**(9), 2013, pp. 11215–11226.
[22] HUA YANG, QILIN ZENG, HUI HU, BOYAN WANG, WEIBIN WANG, *Impact of chirp on soliton trapping of dispersive waves in photonic crystal fiber with two zero dispersive wavelengths*, Optics Communications **325**, 2014, pp. 170–174.
[23] JIAXIN YU, FUHONG CAI, YE WANG, ZHONG CHEN, JINGYUN HUANG, ZHIZHEN YE, JUN QIAN, *Supercontinuum pulse measurement by $KNbO_3$ nanoneedle based cross-correlation frequency-resolved optical gating (XFROG)*, Optical and Quantum Electronics **47**(5), 2015, pp. 1083–1089.
[24] BACHE M., BANG O., ZHOU B.B., MOSES J., WISE F.W., *Optical Cherenkov radiation by cascaded nonlinear interaction: an efficient source of few-cycle energetic near- to mid-IR pulses*, Optics Express **19**(23), 2011, pp. 22557–22562.
[25] LADÁNYI L., SCHOLTZ L., MÜLLEROVÁ J., *Numerical simulations of dispersion effects in chirped Gaussian and soliton pulses*, Optical and Quantum Electronics **49**(3), 2017, article ID 105.
[26] MUSSOT A., BEAUGEOIS M., BOUAZAOUI M., SYLVESTRE T., *Tailoring CW supercontinuum generation in microstructured fibers with two-zero dispersion wavelengths*, Optics Express **15**(18), 2007, pp. 11553–11563.
[27] HERRMANN J., GRIEBNER U., ZHAVORONKOV N., HUSAKOU A., NICKEL D., KNIGHT J.C., WADSWORTH W.J., RUSSELL P.ST.J., KORN G., *Experimental evidence for supercontinuum generation by fission of higher-order solitonsin photonic fibers*, Physical Review Letters **88**(17), 2002, article ID 173901.
[28] EFIMOV A., TAYLOR A.J., OMENETTO F.G., YULIN A.V., JOLY N.Y., BIANCALANA F., SKRYABIN D.V., KNIGHT J.C., RUSSELL P.ST.J., *Time-spectrally-resolved ultrafast nonlinear dynamics in small-core photonic crystal fibers: experiment and modelling*, Optics Express **12**(26), 2004, pp. 6498–6507.
[29] DUDLEY J.M., XUN GU, LIN XU, KIMMEL M., ZEEK E., O'SHEA P., TREBINO R., COEN S., WINDELER R.S., *Cross-correlation frequency resolved optical gating analysis of broadband continuum generation in photonic crystal fiber: simulations and experiments*, Optics Express **10**(21), 2002, pp. 1215–1221.
[30] TARTARA L., CRISTIANI I., DEGIORGIO V., *Blue light and infrared continuum generation by soliton fission in a microstructured fiber*, Applied Physics B **77**(2–3), 2003, pp. 307–311.

[31] HUA ZHANG, SONG YU, JIE ZHANG, WANYI GU, *Effect of frequency chirp on supercontinuum generation in photonic crystal fibers with two zero-dispersion wavelengths*, Optics Express **15**(3), 2007, pp. 1147–1154.

[32] SKRYABIN D.V., GORBACH A.V., *Colloquium: looking at a soliton through the prism of optical supercontinuum*, Reviews of Modern Physics **82**(2), 2010, pp. 1287–1299.

[33] EFIMOV A., YULIN A.V., SKRYABIN D.V., KNIGHT J.C., JOLY N., OMENETTO F.G., TAYLOR A.J., RUSSELL P., *Interaction of an optical soliton with a dispersive wave*, Physical Review Letters **95**(21), 2005, article ID 213902.

[34] KLAUS M., SHAW J.K., *Influence of pulse shape and frequency chirp on stability of optical solitons*, Optics Communications **197**(4–6), 2001, pp. 491–500.

Received May 11, 2017